PAPER

Autoclave-free ultra-early strength concrete preparation using an early strength agent and microstructure properties

Daosheng Sun,[ab] Ziwen Wang,[a] Rui Ma, [ID] *[ab] Aiguo Wang[ab] and Gaozhan Zhang[ab]

In this study, nano calcium silicate hydrate was used as an early strength agent to promote the compressive strength of concrete at 1 day. The strength development and the microstructure of standard concrete (SC), autoclave-free ultra-early strength concrete (ESC) and autoclaved concrete (AC) were comparatively studied. The development of hydration products, morphology and pore-structure with ages were investigated *via* XRD, TG, microhardness, SEM and NMR tests to reveal the mechanism of early strength of ESC. The results showed that the compressive strength of ESC at day 1 achieved 60% of the designed strength, as strong as 45.6 MPa, and only 3% less than that of SC after 90 days. While the compressive strength of AC was significant increased over 90% of ultimate at 1 day, then slightly raised after that. The hydration products did not changed between ESC and SC, but the content of C−S−H gel, $Ca(OH)_2$ and non-evaporated water of ESC was higher in the same specific age. New hydration products such as hydrogarnet and tobermorite were found in AC under autoclave conditions. The microhardness of the paste and ITZ of ESC were also higher than those of SC. The porosity of ESC at 1 day was larger than that of SC, which was contributed by gel pores (1–10 nm). However, AC with higher ratio of large pores than ESC and SC exhibited the largest porosity. The results proved that nano calcium silicate hydrate as an early strength agent significantly increased the early strength of concrete under autoclave-free conditions. Nano calcium silicate hydrate particles supplied additional nucleus in pores and ITZ, accelerated the formation of C−S−H gel, hardened hydration products, and improved the porosity structure. However, with autoclave curing, the hydration products in AC formed with larger size and higher crystallization, which benefited for early strength. However, the large porosity with large size pores might cause damage.

1. Introduction

Modern concrete has been rapidly developing and upgrading promoted by urbanization in the 21st century.[1,2] With the fast progress, the demand for the construction period and structural design became stricter. Early strength concrete could afford sufficient strength in 1–3 days after casting,[3] which has shown great advantages in improving the structural design and reducing the construction time, and has drawn considerable attention in recent years.[4,5]

The strength of concrete was strongly affected by hydration degree, hydration productions and micro-structure. Under standard curing, the compressive strength of concrete was commonly 30% of ultimate strength at 3 days, and this value grew to 90% at 28 days.[6] To increase the early strength, autoclave curing is a useful method.[7,8] However, autoclave curing consumed large energy, caused environment impact and

expensive cost, and cannot be applied in filed practice. Furthermore, there were still problems for this method. Under autoclave conditions, large amounts of hydration products with high crystallinity and large size were generated in short time and wrapped surround the unreacted cement, limited the forward hydration, and made the concrete more brittle.[9–11] Water vapor violently transferred during autoclave curing, causing weak permeability from larger porosity and more connected pores.[12–14] Hence, the research about early strength concrete with autoclave-free curing was significantly important.

Autoclave-free concrete usually exhibited high early strength using early strength agents. Inorganic agents ($CaCl_2$, $Ca(NO_3)_2$, *etc.*) and organic agents ($C_2H_2O_4Ca$, $C_6H_{15}NO_3$, *etc.*) were frequently used and reported in different studies.[15–19] However, inorganic early strength agents often induced harmful ions, such as $Cl^−$, while organic agents were complex and hard to determine the dosage.[20,21] Some researchers studied nanoparticles, such as nano-SiO_2, nano-$CaCO_3$ and nano calcium silicate hydrate [xCaO·SiO_2·y(H_2O), C−S−H], to accelerate the hydration speed and increase the early strength.[22–25] Alizadeh[26] found that the structure of artificial nano C−S−H was similar to that of hydrated C−S−H gel,

[a]*Anhui Province Engineering Laboratory of Advanced Building Materials, Anhui Jianzhu University, Hefei, 230601, China. E-mail: marui1251@163.com*

[b]*Anhui Province Key Laboratory of Advanced Building Materials, Anhui Jianzhu University, Hefei, 230601, China*

Table 1 The table of chemical composition of cement, fly ash and slag (wt/%)

Material	CaO	SiO_2	Al_2O_3	Fe_2O_3	MgO	Na_2O	SO_3	Loss on ignition
Cement	63.23	19.46	4.53	2.80	2.41	0.13	3.31	2.02
Fly ash	3.85	57.29	20.21	11.73	1.14	0.32	0.39	1.51
Slag	38.25	32.58	15.04	0.3	8.57	—	—	5.26

Table 2 The mix proportion of concrete

Sample	Cement (kg m^{-3})	Fly ash (kg m^{-3})	Slag (kg m^{-3})	Water (kg m^{-3})	Sand (kg m^{-3})	Aggregate (kg m^{-3})	Superplasticizer[a] (%)	Early strength agent (%)
SC	310	75	105	135	620	1200	1.1	0
AC	310	75	105	135	620	1200	1.1	0
ESC	310	75	105	135	620	1200	1.1	4.0

[a] The weight percentage of binders.

which accelerated the hydration speed of C_3S. Wang[22] revealed that nano C–S–H in cement enhanced the hydration process in 24 h, then this accelerated effect was declined after 24 h. The effects of nano C–S–H on the microstructure formation of concrete at early age was important to explain the mechanism of the early high strength. However, the study about these issues is still unclear.

In this study, high performance early strength concrete with designed strength of 70 MPa was prepared *via* the autoclave-free method using nano C–S–H as an early strength agent. The compressive strength at 1 day required over 60% of ultimate. The early strength development was comparatively studied among standard concrete (SC), autoclave-free early strength concrete (ESC) and autoclave concrete (AC). The micro-structure properties were also investigated with phase, content and morphology of hydration products, microhardness and pore structure to reveal the mechanism of the early strength development.

2. Materials and methods

P·II52.5 Portland cement,[27] class F fly ash (FA) and S95 granular blast furnace slag were used as binder materials in this research. The chemical compositions of binders are listed in Table 1. Fine aggregate was river sand with the modulus of 2.58. Stone with continuous grade from 5 mm to 19.5 mm was used as coarse aggregate. A PE-200 polycarboxylate superplasticizer and composite nano C–S–H early strength agent (SBT-511) were utilized to improve the properties. The dosage of the early strength agent and the polycarboxylate superplasticizer was 4.0% and 1.1% of the total cementitious material, respectively. The mix proportions are shown in Table 2.

For mix preparation, binder materials were firstly stirred for 1 min, and then fine and coarse aggregates were added separately and mixed for another 2 min. Lastly, water and chemical agent were added and stirred for 5 min until a uniform mixture
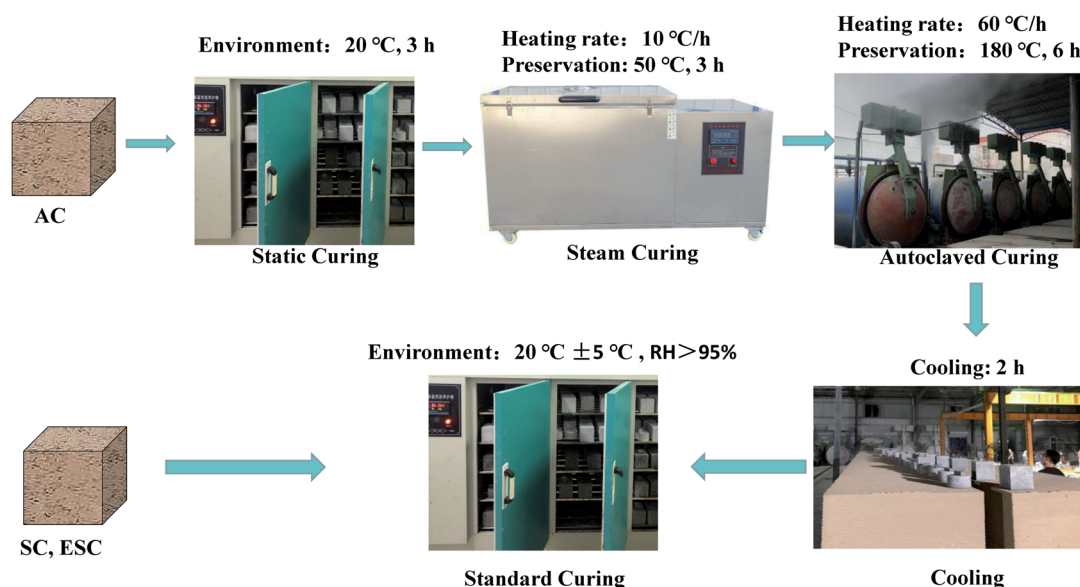

Fig. 1 Flowchart of the fabrication process of different concrete.

formed. For SC and ESC, the concrete was cured under standard environment (20 °C ± 5 °C, RH > 95%) until specific ages. However, for AC, the concrete was successively steam cured and autoclave cured at the first 8 h after casted, and then cooled and removed into standard environment for designated age. The curing regime for AC is shown as the flow chart in Fig. 1.

The compressive strength of concrete was tested following the Chinese standard "Standard for test method of mechanical properties on ordinary concrete".[28] The specimens with the size of $100 \times 100 \times 100$ mm were compressed by a universal testing machine with the load of 10 kN s^{-1}.

The phase and the content of hydration products were analysed by X-ray diffraction (XRD) and thermogravimetry (TG) method. The paste samples without aggregates were prepared to avoid the disruption of sand and stone. The paste samples were stopped hydration with ethanol at the designated age, then dried under 40 °C for constant weight, and ground into powder to pass the 200-mesh sieve. In the XRD test, the sample was scanned from 5° to 75° at the scanning rate of 10 (°)·min^{-1}.

TG was tested with NETZSCH STA449F3, and the sample was heated from ambient temperature to 1000 °C under nitrogen protection. Several thermal reactions occurred at different temperatures, which included the dehydration of the C–S–H gel (50–600 °C, major at 120 °C), dehydration of aluminate hydrate (110–150 °C), decomposition of Ca(OH)$_2$ (400–430 °C), and decomposition of CaCO$_3$ (650–690 °C).[29,30] With the mass loss curves in TG, the contents of Ca(OH)$_2$ and non-evaporate water were calculated by eqn (1)–(3):[25,31]

$$W_{CH} = W_{400-430} \times \frac{74}{18} + W_{650-690} \times \frac{74}{44} \quad (1)$$

$$W_{n-W} = (W_{105-1000} - L_c)/(1 - L_c) \quad (2)$$

$$L_c = f_{PC} \times L_{PC} + f_{FA} \times L_{FA} + f_S \times L_S \quad (3)$$

where $W_{400-430}$, $W_{650-690}$, and $W_{105-1000}$ are the mass loss percentage between 400–430 °C, 650–690 °C and 105–1000 °C, respectively. L_c, L_{PC}, L_{FA}, an L_S are the mass loss percentages on the ignition of concrete and mineral admixture, and f_{PC}, f_{FA}, and f_S are the mix proportions of the mineral admixture in concrete.

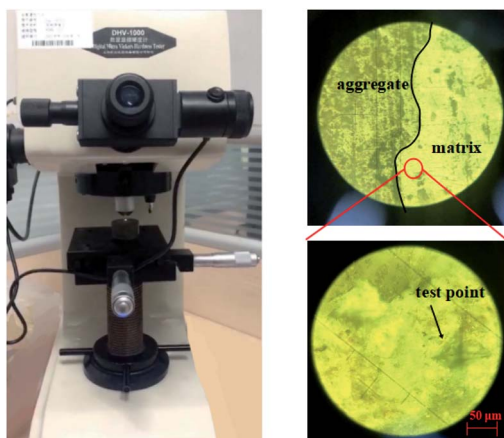Microhardness can reflect the strength of the matrix and interfacial transition zone (ITZ) and a loose ITZ obtained a low microhardness value.[32] The ITZ width can also be evaluated according to the trend of microhardness with the change in distance. In this study, microhardness was tested by a HVS-50 Vickers hardness tester (Fig. 2). By measuring the width of indentations pressed by a diamond indenter, the microhardness was determined according to eqn (4):

$$H_V = \frac{1.854F}{d^2} \quad (4)$$

where F is the load and d is the mean width of indentations. For sample preparation, a concrete specimen with the size of $2 \times 2 \times 2$ cm was immobilized by epoxy resin, and then polished by a sandpaper with different grades of P 400, P 800, P 1200 and P 2000, respectively, to expose a smooth surface of the sample.

The morphology of hydration products in different concretes for ages was observed by a scanning electron microscope (SEM) using a Schottky field emission scanning electron microscope (ZEISS GeminiSEM 500).

The pore structure was test by low field nuclear magnetic resonance (L-NMR). L-NMR is a continuing, non-destructive and high accuracy test method. Its working principle is to quantitatively characterize the content and distribution of pore water, and the interactions between water molecules and pore walls using the relaxation properties of ^{1}H protons in water molecules.[33] The longer the relaxation time is, the larger the pore radius is. Based on the fast exchange theory, the pore size distribution is related to the transverse relaxation time distribution.[34] A New MesoMR12-060V-I spectrometer was used in the experiment. The resonant frequency was 12 MHz, the diameter of the probe coil was 25 mm, and the temperature of the magnet was controlled at 32.00 ± 0.02 °C. The concrete samples with a size of $2 \times 2 \times 2$ cm were vacuum-saturated with distilled water for 24 h before tested.

3. Results and discussion

3.1. Compressive strength development

Fig. 3 shows the development of the compressive strength of SC, ESC and AC with the error bar of standard deviation. The

Fig. 2 HVS-50 Vickers hardness tester and images of tested concrete.
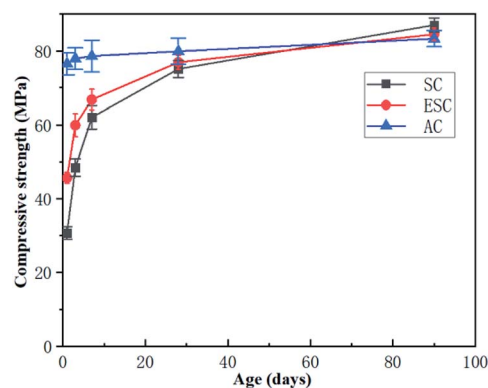

Fig. 3 Strength development with the standard error of 3 groups concrete with ages.
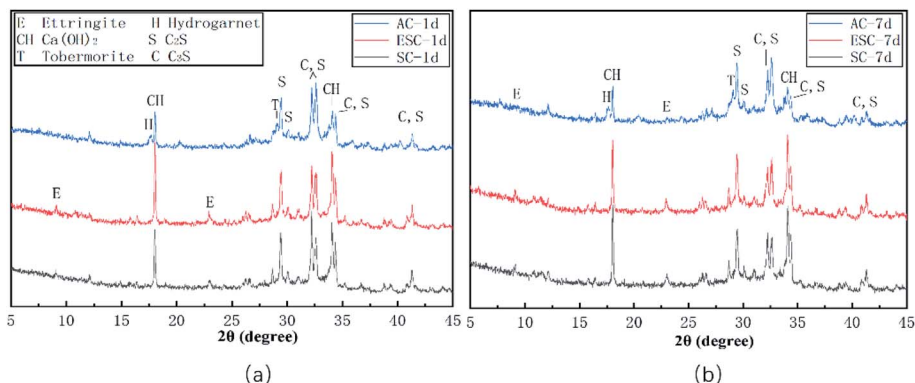
Fig. 4 XRD patterns of SC, ESC and AC pastes for (a) 1 day and (b) 7 days.

strength of concrete at 28 days was nearly the same and all over 75 MPa, but the strength development processes were much different. For SC, the strength at 1, 3 and 7 days were about 40.9%, 64.4%, and 82.6% of it at 28 days, respectively. However, for ESC, the strength at 1 day reached 60.7%, about 45.6 MPa. Compared to that of SC, the strength of ESC increased 48.5%, 23.8% and 7.7% at corresponding age, respectively. However, for AC, the strength at 1 day approximately achieved the value at 28 days, and then the growth was insignificant.

The results demonstrated that nano C–S–H as an early strength agent significantly accelerated the early strength of concrete, and the compressive strength at 1 day developed 60%. Also, the strength of ESC for each age was higher than that of SC, but the increment declined with ages. However, with autoclave curing, the strength of the concrete was mostly contributed during the autoclave period, then the growth of strength was almost negligible, and has shown the weakest strength after 90 days.

3.2. Hydration products

3.2.1. XRD analysis.
The XRD patterns for 3 paste samples cured for 1d and 7d are shown in Fig. 4. The main diffraction peaks for 3 samples were mostly unreacted C_2S and C_3S, and $Ca(OH)_2$. On comparison, in Fig. 4(a), the diffraction peak near 9.1° that belongs to ettringite appeared in SC and ESC, and the intensity of the $Ca(OH)_2$ peak in ESC was much stronger than that in SC. However, no ettringite was found in AC. Instead, there were new peaks from hydrogarnet [$3CaO(Al_2O_3,Fe_2O_3) \cdot$

$6H_2O$] and tobermorite [$Ca_5Si_6O_{16}(OH)_2 \cdot 4H_2O$]. For 7d, in Fig. 4(b), no new products were formed, but the intensity of $Ca(OH)_2$ in SC significantly increased.

The XRD results demonstrated that with autoclave-free curing, there was not any difference in the type of resulted hydration products between ESC and SC, but the content of $Ca(OH)_2$ in ESC at 1d increased due to the rapid hydration rate. These results proved that the early strength agent did not affect the essence but accelerated the reaction. In AC, new products were formed. It was supposed that, under a high temperature and high pressure environment, the ettringite product was decomposed,[35] $Ca(OH)_2$ reacted with Si^{2+} and Al^{3+} to form hydrogarnet,[36,37] C–S–H rich in calcium absorbed dissolved SiO_2 to form tobermorite,[38] and the crystallinity of tobermorite was higher than that of C–S–H. To quantitatively analyse the content of different products in concrete with ages, the TG test was also carried out, and the results are shown in Fig. 5.

3.2.2. TG analysis.
Fig. 5 is the TG curves for hardened paste samples cured for 1d, 3d and 7d, respectively. The different thermal reaction regions were also distinguished with colours. The mass loss percentage in each temperature range was analysed and the content of $Ca(OH)_2$ and non-evaporated water was calculated. The results are listed in Table 3.

The results in Table 3 indicated that, at the same age, the content of $Ca(OH)_2$ and non-evaporated water of ESC were higher than that of SC, and the values for 1d were increased to 13.5% and 12.7%. While for AC, the non-evaporated water was
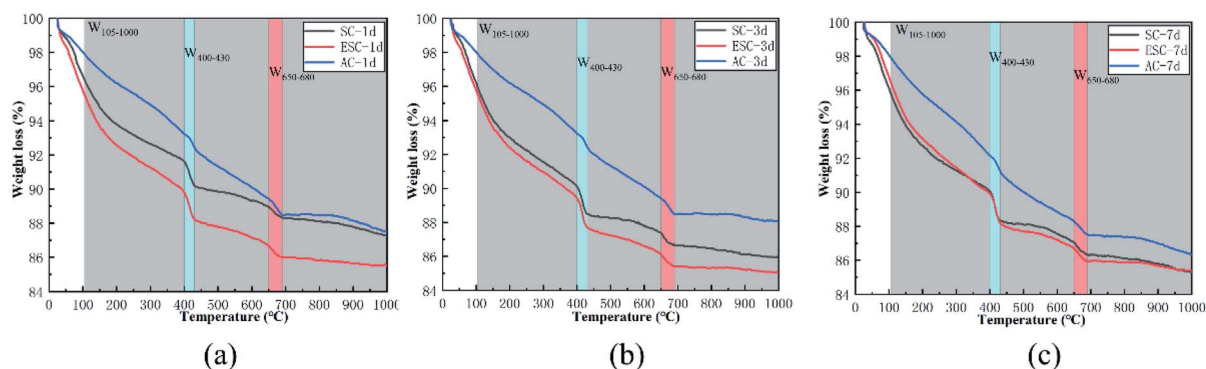

Fig. 5 TG curves of SC, ESC and AC hardened cement pastes cured for (a) 1 day, (b) 3 days and (c) 7 days.

Table 3 The weight losses and the content of Ca(OH)$_2$, non-evaporative water (%) at different ages

Sample	SC-1d	SC-3d	SC-7d	ESC-1d	ESC-3d	ESC-7d	AC-1d	AC-3d	AC-7d
$W_{400-430}$	1.418	1.634	1.722	1.615	1.713	1.755	1.201	1.452	1.555
$W_{650-690}$	0.614	0.696	0.706	0.682	0.705	0.750	0.524	0.647	0.682
$W_{105-1000}$	9.100	9.917	10.519	9.966	10.453	11.039	10.804	11.165	11.558
W_{CH}	6.862	7.888	8.266	7.787	8.226	8.477	5.819	7.057	7.538
W_{n-W}	6.967	7.93	8.605	7.849	8.493	9.023	8.605	8.995	9.394

the most in 1d, and approximately with ESC at 7d, but the content of Ca(OH)$_2$ was much smaller.

In concrete, the content of non-evaporate water can reflect the hydration degree. The results above illustrated that the hydration degree of ESC at a specific age was higher than that of SC. While for AC, although the 1d hydration degree was significantly increased, the dosage of the C–S–H gel and Ca(OH)$_2$ declined. This might because more C–S–H gel and Ca(OH)$_2$ were consumed by the pozzolanic reaction of fly ash and GGBS, and the formation of hydrogarnet and tobermorite under high temperatures.[39] This result also coincided with XRD.

3.2.3. Microhardness analysis. The properties of ITZ were much important for concrete.[40–42] The microhardness at both interfacial transition zone (ITZ) and matrix of concrete at different ages was tested, and the results are shown in Fig. 6. The microhardness for 3 samples at two regions was all increased with age, and the value at matrix was higher than that at ITZ, which revealed ITZ as a weak area for concrete. Unlike SC, the microhardness around paste and ITZ of ESC were also higher especially for 1 day, which was increased to 15.3% and 14.2%, respectively. This result was also coincided with the compressive strength. However, the microhardness of AC was greatly enhanced at 1d, and the growth in the later period was negligible.

Nano C–S–H particles contained in early strength agent dispersed in pore and ITZ, supplying more reaction nucleus. These addition nucleuses accelerated hydration speed at an early age, forming more hydration products to surround reacted cement in short time. The thick products shell limited the growth spaces, and caused more dense products to enhance the microhardness.[43] In another hand, early strength agent promoted the hydration degree of ESC, so that sufficient hydration gel filled the micro pore and ITZ, improved the microhardness, and consequently performed

high early strength. However, for AC, the growth of microhardness was contributed by the large content and highly crystalline of crystal products, which were rarely formed after autoclaved condition. In order to further proved this statement, SEM and NMR test were utilized to investigate the micro-structure.

3.3. Micro-structure of the autoclaved-free early strength concrete

3.3.1. Morphology. Fig. 7 presents the SEM images of hydration products at 1d (a–c) and 7d (d–f) of SC, ESC and AC, respectively. As shown in Fig. 7(a) and (b), only few gel-like products were appeared on the surface of particles in SC, while more amorphous sheet-like C–S–H gel were observed in ESC. In AC of Fig. 7(c), few needle-like products of AFt were found, instead, more crystal-like products with stratified structure were presented and bonded with unreacted cement particles to form a stable skeleton. Unlike C–S–H gel, these stratified structure products were more uniform with high crystallinity, which inferred as tobermorite. This result was also accorded with XRD test. With the age going on, the looser C–S–H gel with needle-sharped was appeared in SC at 7d, but the gel formed in ESC was still packed denser. And in AC, lots of AFt generated under gentle environment.

Nucleation effects of nano C–S–H in ESC preferred to form hydration products with small size and dense packing.[44] Also, nano C–S–H supplied additional Ca^{2+} resources for the C–S–H gel formation, which benefited the dense structure and micro strength of the C–S–H gel. However, the autoclaved environment for AC caused more formation of crystal products, and the staggered crystal helped for the micro-structure stability.

3.3.2. Pore structure. Fig. 8 is the cumulative porosity curve (a) and pore distribution curve (b) at 1d and 7d. It could be found that compared with SC at 1d porosity and gel pore
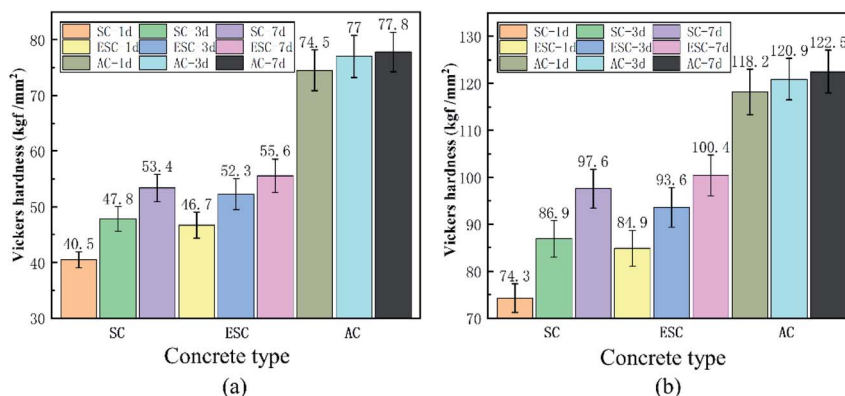
Fig. 6 Microhardness with the standard error of (a) ITZ and (b) matrix of SC, ESC and AC at different ages.
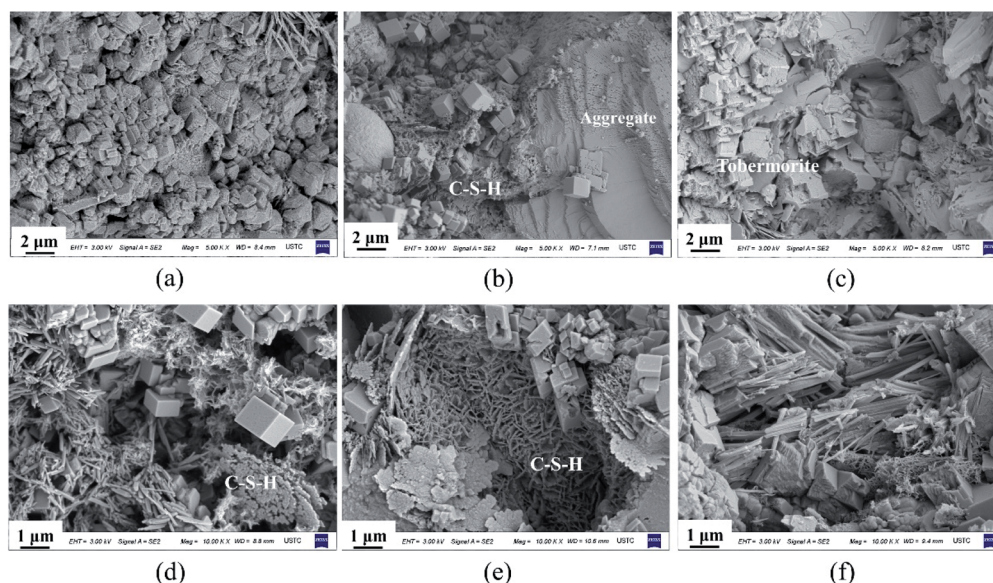
Fig. 7 SEM images of (a) SC at 1 day, (b) ESC at 1 day, (c) AC at 1 day, (d) SC at 7 days, (e) ESC at 7 days, (f) AC at 7 days.
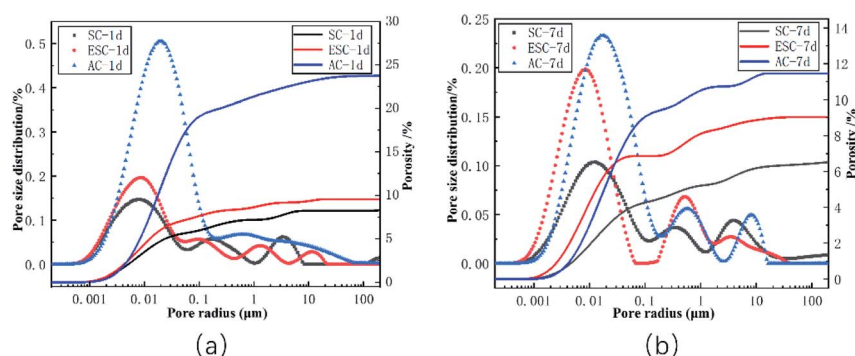

Fig. 8 Accumulative porosity and pore size distribution of SC, ESC and AC (a) at 1 day and (b) at 7 days.

content in ESC were higher, with less pore larger than 100 nm. However, AC performed the highest porosity, which achieved 23.75%, and the pore distribution was more continuous. However, in Fig. 8(b), the pore structures in three concretes were all refined.

Larger gel porosity indicated that more C–S–H gel was formed, and the concrete was further hydrated with higher strength, which was conformed the results of TG and compressive strength tests. When AC was curing, the autoclaved condition caused water vapor transferred in concrete intensely, making more connected large pores, which were detrimental for permeability. The early high strength of AC was caused by the stable skeleton of more crystal products with a large size, while the denser C–S–H gel with an improved micro-structure resulted in the high early strength of ESC.

4. Conclusions

(1) The early strength of ESC was significant improved in this research. The compressive strength at 1d reached 45.6 MPa, about 60% of the ultimate value. Then, the development of strength for long term was similar to SC. However, the strength of AC was mostly generated at the autoclaved period, and the growth was negligible after autoclaved curing.

(2) The early strength in ESC did not change the hydration product category, but accelerated the reaction speed. The accelerated effect raised the hydration degree, formed dense C–S–H gel and $Ca(OH)_2$, and improved the microhardness of ITZ and matrix. However, in AC, the C–S–H gel and hydrated aluminate products were transformed into hydrogarnet and tobermorite, with large size and highly crystallinity.

(3) The gel porosity in ESC was higher than that of SC, with the finer pore structure. The porosity of AC at 1d was highest, which about 23.75%.

(4) Nano C–S–H in the early strength agent supplied additional nucleus to accelerate early hydration, forming more C–S–H gel and $Ca(OH)_2$, improving the ITZ structure. Also, products formed preferred small size and denser structure, which supplied high microhardness and consequently increased early strength.

Author contributions

Conflicts of interest

There are no conflicts to declare.

Acknowledgements

References

1 R. Ma, L. P. Guo, S. X. Ye, W. Sun and J. P. Liu, Influence of hybrid fiber reinforcement on mechanical properties and autogenous shrinkage of an ecological UHPFRCC, *J. Mater. Civ. Eng.*, 2019, **31**(5), 04019032.

2 J. Y. Jiang, W. J. Zhou, H. Y. Chu, F. J. Wang, L. G. Wang, T. T. Feng and D. Guo, Design of eco-friendly ultra-high performance concrete with supplementary cementitious materials and coarse aggregate, *J. Wuhan Univ. Technol., Mater. Sci. Ed.*, 2019, **34**(6), 1350–1359.

3 D. Ghosh, A. Abd-Elssamd, Z. J. Ma and D. Hun, Development of high-early-strength fiber-reinforced self-compacting concrete, *Constr. Build. Mater.*, 2021, **266**, 121051.

4 J. Sun, H. Shi and B. Qian, Effects of synthetic CSH/PCE nanocomposites on early cement hydration, *Constr. Build. Mater.*, 2017, **140**, 282–292.

5 Z. Y. Zhou, M. Sofi, J. L. Liu, S. P. Li, A. C. Zhong and P. Mendis, Nano-CSH modified high volume fly ash concrete: early-age properties and environmental impact analysis, *J. Cleaner Prod.*, 2012, **286**, 124924.

6 M. H. Zhang and J. Islam, Use of nano-silica to reduce setting time and increase early strength of concretes with high volumes of fly ash or slag, *Constr. Build. Mater.*, 2012, **29**, 573–580.

7 H. Yazici, E. Deniz and B. Baradan, The effect of autoclave pressure, temperature and duration time on mechanical properties of reactive powder concrete, *Constr. Build. Mater.*, 2013, **42**(9), 53–63.

8 H. Yazici, The effect of curing conditions on compressive strength of ultra high strength concrete with high volume mineral admixtures, *Build. Environ.*, 2007, **42**(5), 2083–2089.

9 F. Cassagnabere, G. Escadeillas and M. Mouret, Study of the reactivity of cement/metakaolin binders at early age for specific use in steam cured precast concrete, *Constr. Build. Mater.*, 2009, **23**(2), 775–784.

10 S. Shaw, S. M. Clark and C. M. B. Henderson, Hydrothermal formation of the calcium silicate hydrates, tobermorite ($Ca_5Si_6O_{16}(OH)_2 \cdot 4H_2O$) and xonotlite ($Ca_6Si_6O_{17}(OH)_2$): an *in situ* synchrotron study, *Chem. Geol.*, 2000, **167**, 129–140.

11 H. Salahuddin, L. A. Qureshi, A. Nawaz, M. Abid, R. Alyousef, H. Alabduljabbar, F. Aslam, S. F. Khan and R. F. Tufail, Elevated temperature performance of reactive powder concrete containing recycled fine aggregates, *Materials*, 2020, **13**(17), 26.

12 Z. Y. Liu, L. K. Bu, Z. X. Wang and G. Q. Hu, Durability and microstructure of steam cured and autoclaved PHC pipe piles, *Constr. Build. Mater.*, 2019, **209**, 679–689.

13 S. Q. Tian, L. W. Fan, Z. T. Yu and J. Ge, A fractal model on predicting the water vapor permeability of autoclave aerated concrete (AAC) with various porosities, *Int. J. Heat Mass Transfer*, 2020, **149**, 119563.

14 C. Ma, G. Yi, G. C. Long and Y. J. Xie, Properties of high-early-strength aerated concrete incorporating metakaolin, *J. Mater. Civ. Eng.*, 2019, **31**(10), 04019225.

15 G. D. Schutter and L. Luo, Effect of corrosion inhibiting admixtures on concrete properties, *Constr. Build. Mater.*, 2004, **18**(7), 483–489.

16 K. Y. Ann, H. S. Jung and H. S. Kim, Effect of calcium nitrite-based corrosion inhibitor in preventing corrosion of embedded steel in concrete, *Cem. Concr. Res.*, 2006, **36**(3), 530–535.

17 M. S. Zhang, Preparation and mechanism analysis of high-efficiency early strength agent, *Adv. Mater. Res.*, 2012, **2483**, 535–537.

18 M. Heikal, Effect of calcium format as an accelerator on the physicochemical and mechanical properties of pozzolanic cement pastes, *Cem. Concr. Res.*, 2004, **34**(6), 1051–1056.

19 S. W. Son and J. H. Yeon, Mechanical properties of acrylic polymer concrete containing methacrylic acid as an additive, *Constr. Build. Mater.*, 2012, **37**(12), 669–679.

20 K. F. Tan and J. Z. Zhu, Influences of steam and autoclave curing on the strength and chloride permeability of high strength concrete, *Mater. Struct.*, 2017, **50**(1), 56.

21 J. Wang, C. X. Qian, J. Qu and J. Q. Guo, Effect of lithium salt and nano nucleating agent on early hydration of cement based materials, *Constr. Build. Mater.*, 2018, **174**, 24–29.

22 H. Q. Wang, S. G. Zhang and B. N. Wu, Experimental study on selection of early-strength agent for low-strength cementitious materials prepared with manganese tailings, *Environ. Earth Sci.*, 2018, **77**(6), 231.

23 G. Land and D. Stephan, Controlling cement hydration with nanoparticles, *Cem. Concr. Compos.*, 2015, **57**, 64–67.

24 K. P. Bautista-Gutierrez, A. L. Herrera-May, J. M. Santamaria-Lopez, A. Honorato-Moreno and S. A. Zamora-Castro, Recent progress in nanomaterials for modern concrete

infrastructure: advantages and challenges, *Materials*, 2019, **12**(21), 3548.

25 R. Ma, L. P. Guo, W. Sun, J. P. Liu and J. Y. Zong, Strength-enhanced ecological ultra-high performance fibre-reinforced cementitious composites with nano-silica, *Mater. Struct.*, 2017, **50**(2), 166.

26 R. Alizadeh, L. Raki, J. M. Makar, J. J. Beaudoin and I. Moudrakovski, Hydration of tricalcium silicate in the presence of synthetic calcium–silicate–hydrate, *J. Mater. Chem.*, 2009, **19**(42), 7937–7946.

27 GB 175-2007, *Standard For Common Portland Cement*, China State Bureau of Quality and Technical Supervision, 2007.

28 GB/T50081-2016, *Standard For Test Method of Mechanical Properties on Ordinary Concrete*, China State Bureau of Quality and Technical Supervision, 2016.

29 R. Masoudi and R. D. Hooton, Examining the hydration mechanism of supersulfated cements made with high and low-alumina slags, *Cem. Concr. Compos.*, 2019, **103**, 193–203.

30 T. Y. Ni, W. B. Ma, Y. Yang, J. R. Yu, J. T. Liu, C. H. Jiang and C. P. Gu, Interface reinforcement and a new characterization method for pore structure of pervious concrete, *Constr. Build. Mater.*, 2021, **267**, 121052.

31 M. Wu, Y. S. Zhang, G. J. Liu, Z. T. Wu, Y. G. Yang and W. Sun, Experimental study on the performance of lime-based low carbon cementitious materials, *Constr. Build. Mater.*, 2018, **168**, 780–793.

32 M. A. Masoud, A. M. El-Khayatt, W. A. Kansouh, K. Sakr, M. G. Shahien and A. M. Zayed, Insights into the effect of the mineralogical composition of serpentine aggregates on the radiation attenuation properties of their concretes, *Constr. Build. Mater.*, 2020, **263**, 120141.

33 L. Liu, Z. He, X. H. Cai and S. J. Fu, Application of low-field NMR to the pore structure of concrete, *Appl. Magn. Reson.*, 2021, **52**, 15–31.

34 F. Wang, X. M. Kong, L. F. Jiang and D. M. Wang, The acceleration mechanism of nano-C–S–H particles on OPC hydration, *Constr. Build. Mater.*, 2020, **249**, 118734.

35 H. F. W. Taylor, C. Famy and K. L. Scrivener, Delayed ettringite formation, *Cem. Concr. Res.*, 2001, **31**(5), 683–693.

36 A. Skawinska, Z. Owsiak, T. Baran and K. Hernik, The influence of halloysite addition on tobermorite formation in CaO and quartz mix under hydrothermal conditions, *Cem.-Wapno-Beton*, 2017, **22**(5), 426–434.

37 X. L. Qiu, Z. G. Zhao and X. G. Zhao, Microstructure and characterization of aluminum-incorporated calcium silicate hydrates (C–S–H) under hydrothermal conditions, *RSC Adv.*, 2018, **8**(49), 28198–28208.

38 Q. Y. Zhao, C. Cui, B. He and X. F. Ding, Investigation of the mechanism of slow hydration in low w/c ratio RPC matrix under long-term autoclaved curing, *Constr. Build. Mater.*, 2020, **237**, 117660.

39 S. Y. Hong and F. P. Glasser, Phase relations in the CaO–SiO_2–H_2O system to 200 °C at saturated steam pressure, *Cem. Concr. Res.*, 2004, **34**, 1529.

40 M. A. Masoud, A. M. Rashad, K. Sakr, M. G. Shahien and A. M. Zayed, Possibility of using different types of Egyptian serpentine as fine and coarse aggregates for concrete production, *Mater. Struct.*, 2020, **53**(4), 1–17.

41 A. M. Zayed, M. A. Masoud, M. G. Shahien, H. S. Gökçe, K. Sakr, W. A. Kansouh and A. M. El-Khayatt, Physical, mechanical, and radiation attenuation properties of serpentine concrete containing boric acid, *Constr. Build. Mater.*, 2021, **272**, 121641.

42 A. M. Zayed, M. A. Masoud, A. M. Rashad, A. M. El-Khayatt, K. Sakr, W. A. Kansouh and M. G. Shahien, Influence of heavyweight aggregates on the physico-mechanical and radiation attenuation properties of serpentine-based concrete, *Constr. Build. Mater.*, 2020, **260**, 120473.

43 A. Hosan, F. U. A. Shaikh, P. Sarker and F. Aslani, Nano- and micro-scale characterisation of interfacial transition zone (ITZ) of high volume slag and slag-fly ash blended concretes containing nano SiO_2 and nano $CaCO_3$, *Constr. Build. Mater.*, 2021, **269**, 121311.

44 Z. P. Li, J. Gong, S. Du, J. L. Wu, J. F. Li, D. Hoffman and X. M. Shi, Nano-montmorillonite modified foamed paste with a high volume fly ash binder, *RSC Adv.*, 2017, **7**, 9803.